Impurity screening in carbon nanotubes

M. F. Lin[*] and D. S. Chuu

Electrophysics Department, National Chiao Tung University, Hsinchu 30050, Taiwan, Republic of China

(Received 3 January 1997; revised manuscript received 7 April 1997)

Nanotube geometry determines electronic structure and thus impurity screening. A metallic carbon nanotube could effectively screen a charged impurity, while a semiconducting carbon nanotube could not. The ability to screen a long-range Coulomb field is mainly determined by whether there are free carriers in the subbands nearest the Fermi level. The detailed screening properties are sensitive to the impurity position, and the tubular structure (such as radius and chiral angle). Strong, short-wavelength Friedel oscillations at long distances are found to exist only in metallic armchair nanotubes. They are relatively obvious for a smaller armchair nanotube, and could survive at room temperature. [S0163-1829(97)06632-0]

I. INTRODUCTION

Carbon nanotubes have stirred many studies, since they were found in 1991 by Iijima.[1] They are predicted to be metals or semiconductors, depending on radii and chiral angles.[2–4] A single-walled nanotube could be regarded as a rolled-up graphite sheet in cylindrical form. It is characterized by a two-dimensional (2D) vector $\mathbf{R}_x = m\mathbf{a}_1 + n\mathbf{a}_2$,[5] where $\mathbf{a}_1$ and $\mathbf{a}_2$ are primitive lattice vectors of a graphite sheet. A nanotube represented by (m,n) has a radius $r = b\sqrt{3(m^2 + mn + n^2)}/2\pi (b = 1.42$ Å$)$ and a chiral angle $\theta = \tan^{-1}[-\sqrt{3}n/(2m+n)]$. It is a metal (semiconductor) when $2m + n = 3I (\neq 3I$, where I is an integer).[4] For a metallic nanotube, the band gap due to the Peirels distortion[2,6] and the σ-π mixing effect[4] is negligible at room temperature except for a very small zigzag nanotube $(\theta = 0°)$.[4] The band property, metal or semiconductor, will be reflected in most of the physical properties, e.g., the impurity screening, studied here.

The tight-binding model,[4] as employed for a graphite sheet,[7] is used to calculate the π bands formed by $2p_z$ orbitals. A carbon nanotube has many 1D subbands, which are described by the axial wave vectors (k_y's) and discrete angular momenta (J's). A metallic nanotube has linear subbands (denoted by J_a's) intersecting at the Fermi level (Fig. 1); that is, the density of states (DOS) is finite at E_F. The electrons in such subbands behave as free carriers in normal metals, and make an outstanding contribution to the low-frequency or static physical properties. They are thus expected to be capable of completely screening the long-range Coulomb field. On the other hand, a semiconducting nanotube without such free carriers could not effectively screen a charged impurity.

Several theoretical studies on screening properties of carbon nanotubes have been performed. It is predicted that the impurity level in a semiconducting nanotube is a shallow level,[8] and that any nanotube could screen large external electric fields.[9] In this work, screening of a charged impurity is mainly studied at room temperature. The dependence on nanotube geometry (such as radius and chiral angle), impurity position, and temperature (T) is included in the study. The present study could provide a basis for further investi-

gation of screening-related physical properties, such as the impurity level,[8] the residual resistivity,[10] the interaction energy of a charged particle with a carbon nanotube,[11] etc.

Screening properties could be understood from the response function χ or the dielectric function ϵ. The self-consistent-field (SCF) approach,[12] including the band-structure effects, has been used to calculate χ. The band structure directly affects the characteristics of χ and thus the screening properties. Whether a carbon nanotube could screen the long-range Coulomb field is mainly determined by χ [Eq. (3)] at zero momentum ($q = 0$) and angular momentum ($L = 0$). A finite $\chi(q=0, L=0) = 0.031$, which is identified to be due to the linear J_a subbands, is the same for all
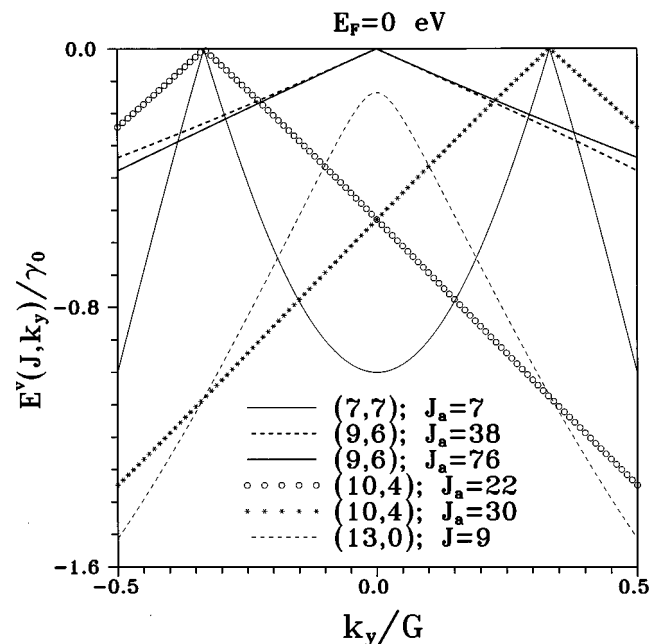

FIG. 1. The energy dispersion relations for the bonding energy bands nearest the Fermi level. They are symmetric, about $E_F = 0$, to the antibonding energy bands. The metallic nanotubes, which include the (7,7), (9,6), and (10,4) nanotubes, have the linear J_a subbands intersecting at $E_F = 0$. However, the semiconducting (13,0) nanotube has the parabolic subband $J = 9$.

metallic nanotubes. However, $\chi(q=0,L=0)$ vanishes in all semiconducting nanotubes. A logarithmic singularity at a finite $q=2k_F$ (k_F is the Fermi momentum) and $L=0$ is further found to exist only in a metallic armchair nanotube [$a(m,m)$ nanotube with $\theta=30°$]. It originates from the excitation between $\pm k_F$ states within the same J_a subband. It is even absent in other metallic chiral nanotubes with finite k_F's, owing to the lack of reflection symmetry. Such a singular structure could cause strong, short-wavelength Friedel oscillations at long distances. The dependence of Friedel oscillations on impurity position, nanotube radius, and temperature will be investigated. The above-mentioned characteristics of χ clearly illustrate that the band structure plays an important role in impurity screening.

This paper is organized as follows. The relation between the π band and the static response function is discussed in Sec. II. Screening properties of carbon nanotubes are studied in Sec. III. Concluding remarks are given in Sec. IV.

II. STATIC RESPONSE FUNCTION

The π band is briefly reviewed as follows. It is calculated using the nearest-neighbor tight-binding Hamiltonian.[7,4] The energy dispersions of the (m,n) nanotube are

$$E^{c,v}(k_x,k_y)=\pm\gamma_0\left\{1+4\,\cos\left(\frac{3b(k_y\cos\theta+k_x\sin\theta)}{2}\right)\right.$$
$$\times\cos\left(\frac{\sqrt{3}b(k_y\sin\theta-k_x\cos\theta)}{2}\right)$$
$$\left.+4\,\cos^2\left(\frac{\sqrt{3}b(k_y\sin\theta-k_x\cos\theta)}{2}\right)\right\}^{1/2},$$

(1a)

and the corresponding wave functions are

$$\Psi^{c,v}(k_x,k_y)=\frac{1}{\sqrt{2}}\left\{U_1(k_x,k_y)\mp\frac{H_{12}^*(k_x,k_y)}{|H_{12}(k_x,k_y)|}U_2(k_x,k_y)\right\}.$$

(1b)

The superscripts c and v, respectively, represent the antibonding ($E\geq0$) and bonding energy bands. They, as shown in Fig. 1, are symmetric to each other about the Fermi level $E_F=0$. The transverse wave vector obtained from the periodic boundary condition is $k_x=J/r$, where $J=1,2,\ldots,N_u/2$; N_u is the atom number in a primitive unit cell.[5] The angular momentum J could serve as the subband index. The axial wave vector k_y is confined within the first Brillouin zone. U_1 and U_2 are the two tight-binding functions, and H_{12} is the nearest-neighbor Hamiltonian matrix element. The resonance integral $\gamma_0=3.033$ eV is taken in this work.[4]

The geometric structure uniquely determines the electronic structure and thus the impurity screening. There are three main characteristics in the π-band structure. First, a metallic (m,n) nanotube, with $2m+n=3I$, has linearly dispersive antibonding and bonding bands intersecting at $E_F=0$. The J_a subbands are described by the dispersion relations $\pm v_f|k\pm k_F|$ ($v_f=3\gamma_0b/2$). The carriers in such subbands would behave like conduction electrons in normal
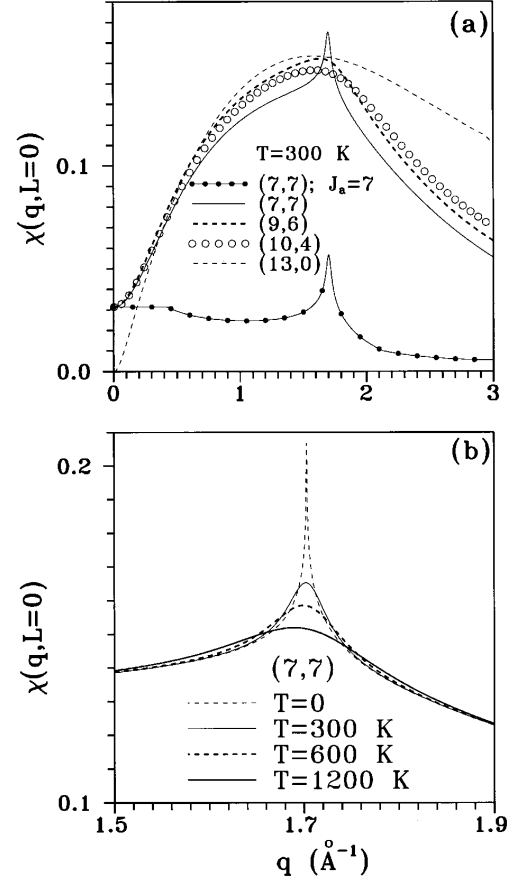

FIG. 2. (a) The static response function $\chi(q,L=0)$ for various nanotubes is calculated at room temperature. Also shown for comparison is that from the linear $J_a=7$ subband in the (7,7) nanotube. (b) $\chi(q,L=0)$ of the (7,7) nanotube exhibits a singular structure at $q=2k_F$, which is displayed at various temperatures.

metals due to the finite DOS at $E_F=0$. The free carrier number per area (D) is inversely proportional to radius. On the other hand, a semiconducting nanotube has an energy gap $E_g\propto1/r$.[13] For example, the (7,7), (9,6), and (10,4) nanotubes are metals (Fig. 1), and the (13,0) nanotube is a semiconductor with $E_g=0.82$ eV. Second, a metallic nanotube has a finite (vanishing) Fermi momentum $k_F=\pm G/3$, if $n-m$ is equal (unequal) to $3dI$.[14] G is the reciprocal-lattice vector, and d is the highest common divisor of m and n. For example, k_F of the (7,7) and (10,4) nanotubes is $G/3$, and that of the (9,6) nanotube is zero. A metallic nanotube exhibits a finite χ and $q=0$ and $L=0$, which is demonstrated to be mainly due to the excitations from the states near k_F [Eq. (3)]. The finite $\chi(q=0,L=0)$ contrasts strongly with the vanishing $\chi(q=0,L=0)$ in a semiconducting nanotube. The value of $\chi(q=0,L=0)$ determines whether a carbon nanotube could screen a charged impurity. Finally, carbon nanotubes exhibit the reflection symmetry $E(J,k_y)=E(J,-k_y)$ when the hexagons are arranged along the tubular axis in a nonhelical fashion. They include both armchair nanotubes and zigzag nanotubes, e.g., the (7,7) and (13,0) nanotubes. Hence only an armchair nanotube has finite Fermi momenta, $k_F=\pm G/3$, in the same linear subband J_a. This means that a (m,m) nanotube could exhibit the excitation between $\pm k_F$ states within the same J_a subband. Such a kind of excitation

would lead to a singular structure in $\chi(q=2k_F, L=0)$ [Figs. 2(a) and 2(b)] and thus Friedel oscillations (Figs. 5 and 6).

The π-band structure is included in the calculation of dielectric function via the SCF approach.[12] The static $\epsilon(q,L)$ of a single-walled carbon nanotube is given by[15]

$$\epsilon(q,L) = \epsilon_0 - V(q,L)\chi(q,L), \quad (2a)$$

$$\chi(q,L) = 2 \sum_{h,h'=c,v} \sum_J \int_{1stBZ} \frac{dk_y}{(2\pi)^2}$$

$$\times |\langle J+L, k_y+q; h'|e^{iqy}e^{iL\phi'}|J, k_y; h\rangle|^2$$

$$\times \frac{f[E^{h'}(J+L, k_y+q)] - f[E^h(J,k_y)]}{E^{h'}(J+L, k_y+q) - E^h(J,k_y)}, \quad (2b)$$

where

$$|\langle J+L, k_y+q; h'|e^{iqy}e^{iL\phi}|J, k_y; h\rangle|^2$$

$$= \frac{1}{4}\left\{1 + \left[\frac{q^2 + (L/r)^2}{36}\right]\right\}^{-6}$$

$$\times \left|1 \pm \frac{H_{12}(J+L, k_y+q)H_{12}^*(J,k_y)}{|H_{12}(J+L, k_y+q)H_{12}^*(J,k_y)|}\right|^2. \quad (2c)$$

$\epsilon_0 = 2.4$ is the background dielectric constant due to all excitations outside the π band.[16] $V(q,L) = 4\pi e^2 I_L(qr)K_L(qr)$ is the Coulomb interaction of a 1D electron gas (EGS), where $I_L(K_L)$ is the first (second) kind of modified Bessel function of order L. f is the Fermi-Dirac function. The electron-electron interaction in a carbon nanotube includes two parts: $V(q,L)$ and a transition matrix element between h and h' bands in Eq. (2c) + and − in Eq. (2c), respectively, correspond to $h=h'$ and $h \neq h'$. The transition matrix element is calculated from the band structure, which is very important in determining the static response function.

The main features in impurity screening are closely related to the response function of the $L=0$ excitations (Sec. III). The q dependence of the static response function $\chi(q, L=0)$ is shown in Fig. 2(a) for various nanotubes at room temperature. The effect of temperatures on χ is generally weak except for the singular structure in an armchair nanotube [Fig. 2(b)]. The excitations from the bonding to the antibonding energy bands ($v \rightarrow c$), the only excitation channel at $T=0$, would uniquely determine the principal difference between semiconducting and metallic nanotubes. For semiconducting nanotubes, the $v \rightarrow c$ Coulomb interactions [Eq. 2(c)] vanish at $q=0$ and $L=0$, and so does $\chi(q=0, L=0)$, e.g., the (13,0) nanotube (the light dashed curve). On the other hand, all metallic nanotubes have the same $\chi(q=0, L=0) = 2/\pi^2 v_f = 0.031$. The finite value originates from the linear dispersion of J_a subbands, since the $v \rightarrow c$ Coulomb interactions may exist in these subbands, but not in other subbands. For example, $\chi(q=0, L=0)$ of the (7,7) nanotube is due to the linear subband $J_a = 7$ (the solid-circled curve). In addition, other subbands contribute to $\chi(L=0)$ at $q \neq 0$, so that they would modify the short-range

screening properties. The finite value of $\chi(q=0, L=0)$ could be derived from the expression

$$\chi(q \rightarrow 0, L=0)$$

$$= \frac{2}{\pi^2} \int_{-q+k_F}^{k_F} \frac{dk_y}{v_f|k+q-k_F| + v_f|k-k_F|}. \quad (3)$$

The contributions from the spin, Eq. (2) and the degeneracy of J_a, Eq. (2) (or the states near the finite $\pm k_F$) have been included in Eq. (3). Furthermore, the transition matrix element in Eq. 2(c) is equal to 1 (0) for the left-hand (right-hand) states of $k=k_F$.

The value of $\chi(L=0)$ at $q=0$ is the same for all metallic nanotubes; that at $q=2k_F$, however, might be quite different. An armchair nanotube would exhibit an obvious peak structure at $q=2k_F=1.703$ Å^{-1}, e.g., the (7,7) nanotube [the light solid curve in Fig. 2(a)]. It is caused by the $v \rightarrow c$ excitation between $\pm k_F$ states within the same linear subband J_a. Other chiral nanotubes, with finite k_F's, do not exhibit such a singular structure because of the absence of reflection symmetry, e.g., χ of the (10,4) nanotube [circles in Fig. 2(a)]. The singular structure at $T=0$ is a logarithmic divergence [the light dashed curve in Fig. 2(b)]. It can be obtained from the expression

$$\chi(q \rightarrow 2k_F, L=0) \propto \int \frac{dk_y}{v_f|k+q-k_F| + v_f|k+k_F|}, \quad (4)$$

where the upper or the lower limit of the dk_y integration includes the $-k_F$ state. The logarithmic singularity becomes a peak structure as T increases, and disappears at high temperatures [e.g., $T \gtrsim 1200$ K for the (7,7) nanotube]. It is less apparent for a larger armchair nanotube, and is more easily blurred by the increasing T. Generally speaking, an armchair nanotube with $r < 30$ Å could exhibit a singular structure at $T \lesssim 300$ K.

The aforementioned singular structure deserves a closer examination. Within the tight-binding model, the π-band states of a carbon nanotube are sampled from those of a graphite sheet, i.e., they are derived from the states inside the hexagonal Brillouin zone.[5] The $+k_F$ and $-k_F$ states in an armchair nanotube, respectively, come from the two neighboring corners, the K and K' points. The excitation between $\pm k_F$ states thus corresponds to the intervalley excitation, the $K \rightarrow K'$ excitation, in a graphite sheet. The similar logarithmic divergence at $T=0$ could also be found in a 1D EGS,[17] which suggests that there exists a Peierls transition. Here an armchair nanotube might change from a metal into a semiconductor with a very narrow energy gap. The mean-field transition temperature (T_c) of a small armchair nanotube is estimated to be much lower than room temperature.[3] Moreover, T_c is very rapidly reduced as the nanotube radius increases.[6] In general, the effect due to Peierls transition on the electronic properties is predicted to be negligible even at low temperature.

III. IMPURITY SCREENING

The dielectric function in Eq. (2a) is used to study the screening properties, mainly the effective potential and the induced charge distribution. They are calculated for various nanotubes, with one charged impurity at the center or the surface. The effect due to temperatures is also investigated.

The ionized impurities may come from the substitutional

atoms (e.g., borons and nitrogens),[6] the intercalant atoms (e.g., the alkali-metal atoms), and the incident charged particles (e.g., the positrons).[11] A large concentration of K and Rb has been successfully intercalated into a carbon nanotubes,[18] and electrons are suggested to be transferred from the former to the latter.[19] The impurity screening studied here is suitable for the dilute intercalation, but not the above-mentioned dense intercalation.[18] Let us first consider a single-walled carbon nanotube including one charged impurity Ze at $(R=\gamma_{im}, \phi=0°, y=0)$ (the cylindrical coordinate). The charged impurity produces an external Coulomb interaction, $V^{ex}(q,L)=4\pi Ze^2 I_L(qr_<)K_L(qr_>)$ [$r_<(r_>)$ the smaller (larger) of r and r_{im}], on the (m,n) nanotube. Electrons on the carbon nanotube would screen this external potential. The effective potential and the induced charge density within the SCF approach are given by $V^{eff}(q,L)=V^{ex}(q,L)/\epsilon(q,L)$ and $n^{in}(q,L)=\chi(q,L)V^{eff}(q,L)$. The real-space effective potential is obtained by the inverse Fourier transform

$$V^{eff}(\phi,y)=\frac{1}{4\pi^2}\sum_{L=-\infty}^{+\infty}e^{iL\phi}\int_{-\infty}^{+\infty}e^{iqy}V^{ef}(q,L)dq. \quad (5)$$

A similar relation holds true for the induced charge density $n^{in}(\phi,y)$. The total induced charges are given by $V^{eff}(q,L)\chi(q,L)$ at $q=0$ and $L=0$. They are equal to $-Ze(0)$ for a finite (vanishing) $\chi(q=0,L=0)$, since the Coulomb interaction is logarithmically divergent there. This result implies that metallic and semiconducting nanotubes are, respectively, able and unable to screen the long-range Coulomb field. It is also a good indication of the validity of the calculated response function for carbon nanotubes.

The valence of the charged impurity is taken as $Z=\pm 1$ in the following calculations. The effective potential in Eq. (5) strongly depends on the impurity position. The $r_{im}=0$ case, where a charged impurity is situated at the center of a hollow cylinder, is first examined. The external Coulomb potential for $L=0$, $4\pi e^2 K_{L=0}(qr)$, is the only electric potential; Eq. (5) is thus reduced to

$$V^{eff}(y)=\frac{1}{4\pi^2}\int_{-\infty}^{+\infty}e^{iqy}V^{eff}(q,L=0)dq. \quad (6)$$

The effective potential and the induced charge density are independent of the azimuthal angle ϕ. This result is consistent with the symmetry considerations.

The ratio of $V^{eff}(y)$ to $V^{ex}(y)[=e^2/\sqrt{(r_{im}-r)^2+y^2}]$ is shown in Fig. 3 for various nanotubes. The (7,7) nanotube and the (13,0) nanotube, with similar radii, are taken to illustrate the main difference between metallic and semiconducting nanotubes. V^{eff}/V^{ex} of the (7,7) nanotube (the light solid curve) decreases with y's, while the opposite is true for the (13,0) nanotube (the light dashed curve). Furthermore, the former at long distance approaches zeros approximately in the form $V^{eff}/V^{ex}\propto y^{-1}$, which is in great contrast with the finite value $1/\epsilon_0=0.417$ of the latter (the upper inset in Fig. 3). The long-range Coulomb field is effectively screened by a metallic nanotube, but not a semiconducting nanotube. Metallic nanotubes thus behave as good conductors, and semiconducting nanotubes as dielectrics. The screening ability of a metallic nanotube results from the free carriers in the J_a
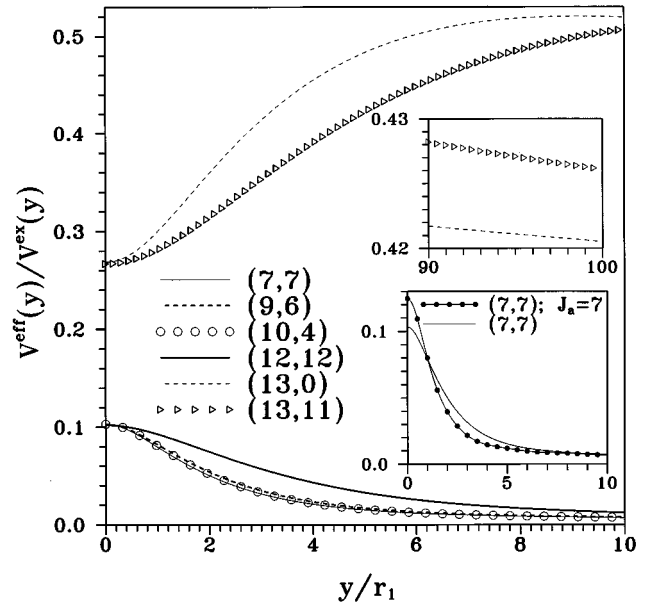

FIG. 3. The ratio of the effective potential vs the external potential is shown for various nanotubes, with a charged impurity at the center (the $r_{im}=0$ case). The upper inset shows $V^{eff}(y)/V^{ex}(y)$ at very large y's for the semiconducting nanotubes, (13,0) and (13,11). That corresponding to the linear $J_a=7$ subband in the (7,7) nanotube is also displayed in the lower inset for comparison. $r_1=4.75$ Å is the radius of the (7,7) nanotube, here and henceforth.

subbands, since the large-y behavior of $V^{eff}(y)$ principally reflects the small-q characteristic of $\chi(L=0)$. For example, the $J_a=7$ subband of the (7,7) nanotube produces a finite $\chi(L=0)$ at small q's [Fig. 2(a)], so that the free carriers in it have the ability to screen the long-range Coulomb field (the solid-circled curve in the lower inset). Other subbands make a contribution to $\chi(L=0)$ at finite q's, while they only modify the effective potential at short distances. In short, the main difference in screening properties between metallic and semiconducting nanotubes is determined by whether there are free carriers or not.

The detailed screening properties are sensitive to the nanotube radius. The effective potential is almost the same for various metallic or semiconducting nanotubes (various θ's) with similar radii, e.g., metallic nanotubes: (7,7), (9,6), and (10,4). However, the free-carrier density of metallic nanotubes and the energy gap of semiconducting nanotubes are appreciably affected by radius, so does the effective potential. A smaller metallic nanotube has higher D; therefore, V^{eff}/V^{ex} would fall off more quickly, as obtained from the comparison of the (7,7) and (12,12) nanotubes. But for a smaller semiconducting nanotube, V^{eff}/V^{ex} is comparatively high, as shown by the (13,0) and (13,11) nanotubes. The increasing E_g or the stronger binding of valence electrons is the main reason. The short-range screening of the Coulomb field is more efficient for a smaller metallic nanotube—a trend contrary to that of a smaller semiconducting nanotube. This feature is essentially independent of the impurity position. The calculated effective potential would be useful for studying other physical properties, e.g., the impurity level,[8] the elastic scattering between conduction electrons and
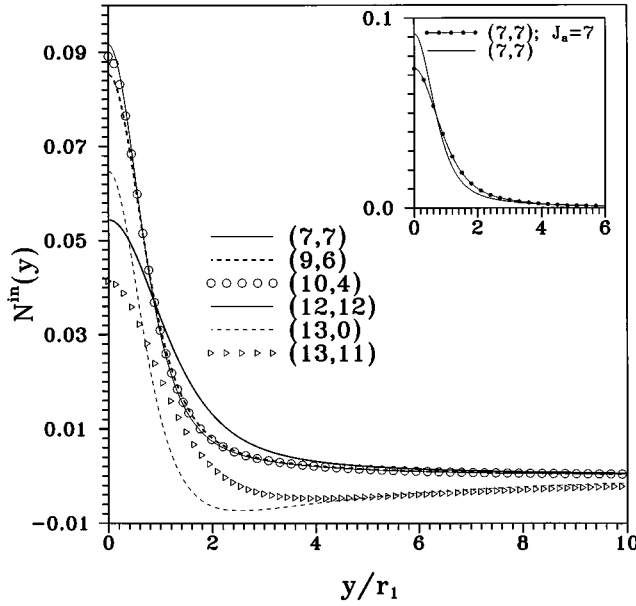
FIG. 4. The induced charge distributions along the tubular axis are shown for various nanotubes. The inset shows the comparison between $N^{in}(y)$ due to all subbands and the $J_a = 7$ subband in the (7,7) nanotube.

charged impurities,[10] and the interaction energy between a carbon nanotube and a charged particle.[11]

The screening charges per unit length, $N^{in}(y) = 2\pi n^{in}(y)$, for the $r_{im} = 0$ case is shown in Fig. 4. For semiconducting nanotubes, the induced charges near a positive charged impurity are electrons, and others are holes, e.g., $N^{in}(y)$ of the (13,0) and (13,11) nanotubes. They are essentially distributed along the tubular axis in a dipolelike form, and the net induced charges are zero. The dipolelike distribution, which weakly reduces the Coulomb field (Fig. 3), is the basic response of valence charges to an external electric field. Such a distribution is comparatively short ranged for a smaller semiconducting nanotube, on account of the larger value of E_g. These results further exemplify the dielectric behavior of semiconducting nanotubes. They also reveal that the transferred charges from the dilute intercalant atoms (e.g., K) would form impurity levels. Such bound states could be further obtained from the effective potential.

There are net screening charges $-Ze$ in a metallic nanotube. The free carriers in the linear subbands J_a's would form a screening cloud to shield the long-range Coulomb field separately, e.g., those in the $J_a = 7$ subband of the (7,7) nanotube (the inset in Fig. 4). Other valence electrons only cause a dipolelike distribution similar to the situation encountered in semiconducting nanotubes. Such a charge distribution further makes the screening charges piled up closer to the charged impurity. It also reduces the effective potential at small y's (the lower inset in Fig. 3); however, the falloff of V^{eff}/V^{ex} might become slower. The induced charge distributions exhibit a diffuse behavior at large distances, which is approximately described by $y^{-3/2}$. Such a behavior is more obvious than that in a 2D (y^{-2}) (Ref. 20) or 3D (y^{-3}) (Ref. 21) EGS.

The effective screening length (λ) is further used to describe the charge distributions. λ here is chosen to be related to the median of the net screening charges:

$$\int_{-\lambda}^{\lambda} N^{in}(y) dy = \frac{-Ze}{2}. \qquad (7)$$

λ is sensitive to radii, but not chiral angles. It is above 3.4 and 5.7 Å, respectively, for the (7,7) and (12,12) nanotubes. The induced charge distributions are relatively extended for a larger metallic nanotube, owing to the lower free-carrier density. The characteristic length is also useful in understanding under what condition the impurity distribution is dilute. Impurities are indicated to be distributed in a dilute manner, when the average distance among impurities is much larger than λ. Their correlations are generally weak under such a condition.

When the impurity position is changed from the center to the surface, the screening properties become complex because of the dependence on azimuthal angle. The average of ϕ's here is taken to simplify the problem. That is to say, the $L = 0$ excitations, as expressed in Eq. (6), are the only contribution to the impurity screening. Such an average is based on the following reasons: (i) If all $L \neq 0$ excitations are taken into consideration, the numerical calculations of the multidimensional integration in Eqs. (2b) and (5) will be difficult to be managed. Some of them are calculated, and their contributions to screening properties are smaller than those of the $L = 0$ excitations. (ii) Impurities, for example, borons and nitrogens, on a carbon nanotube might be distributed in a random and dilute manner. The above approximation is suitable for such kind of impurity distribution. (iii) The essential screening features are expected to remain unchanged, since they are principally dominated by the $L = 0$ excitations. For example, the ability to screen the long-range Coulomb field depends only on the $L = 0$ excitations of the free carriers in the linear J_a subbands.

The effective potential for the $r_{im} = r$ case is also calculated from Eq. (6), but with the external Coulomb potential $4\pi e^2 I_L(qr) K_L(qr)$. It is shown in Fig. 5(a) for various metallic nanotubes. $V^{eff}(y)/V^{ex}(y)$ is equal to zero at $y \to 0$, because the integrand $V^{eff}(q, L=0)$ in Eq. (6) is a well-behaved function at any q. The vanishing value quite differs from the finite value (1) in a 2D or 3D EGS.[20,21] Metallic nanotubes thus exhibit the 1D screening characteristic.[22] $V^{eff}(y)/V^{ex}(y)$ at short distances is much lower than that in the $r_{im} = 0$ case (Fig. 3), e.g., the (7,7) nanotube. This result could be understood from the induced charge distributions. Most of the screening charges, as shown in Fig. 6, are distributed within a small characteristic length, e.g., $\lambda \sim 0.7$ Å for the (7,7) nanotube. Hence they could screen the Coulomb field very efficiently, i.e., the effective potential falls off quickly.

The screening properties at long distances show a diffuse behavior. The $r_{im} = r$ case is similar to the $r_i = 0$ case except for the armchair nanotubes; that is, $V^{eff}(y) \propto y^{-2}$ and $N^{in}(y) \propto y^{-3/2}$ at large y. The (7,7) and (12,12) nanotubes exhibit another outstanding feature, namely, strong, rapid Friedel oscillations. Such oscillations at large y are derived from the first-derivative singularity of the integrand [Eq. (6)] in the Fourier transform.[23] The singular response function at $q = 2k_F$ and $L = 0$ [Fig. 2(b)] is the cause of the Friedel oscillations. The strong, rapid oscillations with a period of
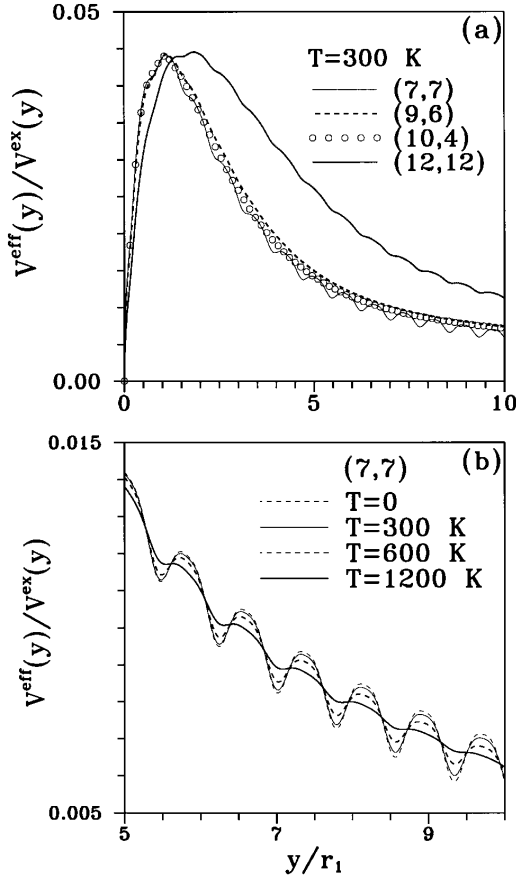
FIG. 5. (a) Similar plot as in Fig. 3, but for the $r_{im}=r$ case. (b) The strong, rapid Friedel oscillations in the (7,7) nanotube is shown at various temperatures.

FIG. 6. A similar plot to that in Fig. 4, but with a charged impurity at the cylindrical surface (the $r_{int}=r$ case). The inset shows the details at large distances. Please notice that $N^{in}(y)$ of the (12,12) nanotube is only shown in the inset for clarity.

$\pi/k_F=3.69$ Å are approximately described by $\sin(2k_F y)/y$ at large y [Fig. 5(b) and the inset in Fig. 6]. It is also noted that the oscillation period is the same for all armchair nanotubes. The Friedel oscillations in armchair nanotubes are similar to those in a 1D EGS.[22] However, they are much stronger than those in a 2D $[\sin(2k_F y)/y^2]$ (Ref. 20) or 3D $[\sin(2k_F y)/y^3]$ (Ref. 21) EGS.

The Friedel oscillations depend on impurity position, nanotube radius, and temperature. The oscillation amplitude should be proportional to the external Coulomb interaction, $4\pi e^2 I_{L=0}(2k_F r_{im})K_{L=0}(2k_F r)$; therefore, it is affected by r_{im} and r. When the impurity is located at the center, the amplitude decays in the exponential form $\exp(-2k_F r)$ because of $2k_F r \gg 1$. This result could explain why Friedel oscillations are absent in the $r_{im}=0$ case (Figs. 3 and 4). It also implies that one charged impurity needs to be close to an armchair nanotube in order to cause the Friedel oscillations. As for the $r_{im}=r$ case, the oscillation amplitude is inversely proportional to r (the inset in Fig. 6). For a smaller armchair nanotube, the Friedel oscillations would be relatively obvious. The singular structure in $\chi(q=2k_F,L=0)$ is gradually broadened by the increasing T [Fig. 2(b)], and the Friedel oscillations behave so [Fig. 5(b)]. The temperature must be sufficiently high to destroy the strong, rapid oscillations thoroughly, e.g., $T \geq 1200$ K for the (7,7) nanotube. Hence the Friedel oscillations in a small armchair nanotube 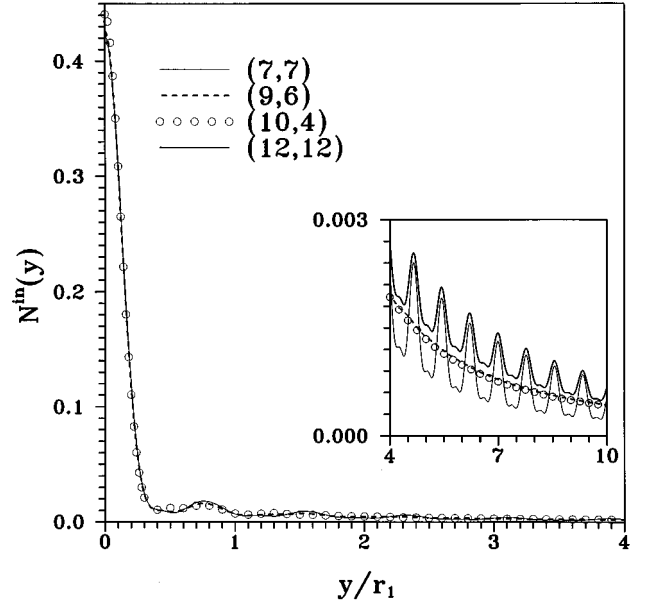are expected to be pronounced at room temperature. The dependence on azimuthal angle is neglected in the above calculations. If the $L \neq 0$ excitations are included in the calculations of Eq. (5), they would somewhat modify the Friedel oscillations for different azimuthal angles. However, the strong, short-wavelength oscillations would remain similar. The Friedel oscillations might affect, e.g., correlations between impurities on a armchair nanotube.

IV. CONCLUDING REMARKS

The impurity screening in carbon nanotubes are studied within the SCF approach. The π-band structure completely dominates the response function and thus the screening properties. χ at $q=0$ and $L=0$ is finite for a metallic nanotube, but vanishing for a semiconducting nanotube. That a metallic nanotube owns the linear subbands intersecting at the Fermi level is the main reason. Hence a metallic carbon nanotube could effectively screen a charge impurity, while a semiconducting carbon nanotube could not. The ability to screen the long-range Coulomb field is determined by whether there are free carriers in the subbands nearest E_F.

The detailed screening properties are strongly affected by the impurity position and the tubular structure. As a result of the higher free-carrier density, the short-range screening is more efficient for a smaller metallic nanotube. The opposite is true for a smaller semiconducting nanotube because of the larger energy gap. Metallic nanotubes, armchair nanotubes excepted, exhibit monotonously diffuse behavior at long distances. Their long-range screening behavior is indicated to be very different from that in a 1D EGS.[22]

For an armchair nanotube, it has finite Fermi momenta and reflection symmetry; therefore, it could exhibit strong, short-wavelength Friedel oscillations. Such oscillations are

relatively obvious for a smaller armchair nanotube, and could survive at room temperature. They are expected to affect the impurity ordering, e.g., borons and nitrogens on an armchair nanotube. A closer investigation in this regard is needed.

The study on impurity screening clearly illustrates the importance of the unique π-band structure. It could provide a basis of understanding for other impurity-related properties. For example, the calculated effective potential could be further used to study the impurity level,[8] the residual resistivity,[10] the electrodynamics of charged particles inside a carbon nanotube,[11] etc.

---

[*]Present addresss: Physics Department, National Cheng Kung University, Tainan 70101, Taiwan, Republic of China.

[1]S. Iijima, Nature (London) **354**, 56 (1991); S. Iijima and T. Ichihashi, *ibid.* **363**, 603 (1993).

[2]J. W. Mintmire, B. I. Dunlap, and C. T. White, Phys. Rev. Lett. **68**, 631 (1992).

[3]N. Hamada, S. I. Sawada, and A. Oshiyama, Phys. Rev. Lett. **68**, 1579 (1992).

[4]R. Saito, M. Fujita, G. Dresselhauss, and M. S. Dresselhauss, Appl. Phys. Lett. **60**, 2204 (1992); Phys. Rev. B **46**, 1804 (1992).

[5]For the details of the nanotube geometry and the π-band structure, see M. F. Lin and K. W.-K. Shung, Phys. Rev. B **52**, 8423 (1995).

[6]N. A. Viet, H. Ajiki, and T. Ando, J. Phys. Soc. Jpn. **63**, 3036 (1994).

[7]P. R. Wallace, Phys. Rev. **71**, 622 (1947).

[8]J. Y. Yi and J. Bernholc, Phys. Rev. B **47**, 1708 (1993).

[9]L. Lou, P. Nordlander, and R. E. Smalley, Phys. Rev. B **52**, 1429 (1995).

[10]Z. Wang, M. Luo, D. Yan, H. Ying, and W. Li, Phys. Rev. B **51**, 13 833 (1995).

[11]V. V. Klimov and V. S. Letokhov, Phys. Lett. A **222**, 424 (1996).

[12]H. Ehrenreich and M. H. Cohen, Phys. Rev. **115**, 786 (1959).

[13]C. T. White, D. H. Robertson, and J. W. Mintmire, Phys. Rev. B **47**, 5485 (1993).

[14]R. A. Jishi, D. Inomata, K. Nakao, M. S. Dresselhaus, and D. Dresselhaus, J. Phys. Soc. Jpn. **63**, 2252 (1994).

[15]M. F. Lin, D. S. Chuu, C. S. Huang, Y. K. Lin, and K. W.-K. Shung, Phys. Rev. B **53**, 15 493 (1996).

[16]E. A. Taft and H. R. Philipp, Phys. Rev. B **138**, A197 (1965).

[17]G. Gruner, *Density Waves in Solids* (Addison-Wesley, New York, 1994).

[18] O. Zou, R. M. Fleming, D. W. Murphy, C. H. Chen, R. C. Haddon, A. P. Ramirez, and S. H. Glarum, Science **263**, 1744 (1994).

[19]Y. Miyamoto, A. Rubio, X. Blase, M. L. Cohen, and S. G. Louie, Phys. Rev. Lett. **74**, 2993 (1995).

[20]F. Stern, Phys. Rev. Lett. **18**, 546 (1967).

[21] G. D. Mahan, *Many-Particle Physics* (Plenum, New York, 1981).

[22] G. Y. Hu and R. F. O'Connell, J. Phys. Condens. Matter **2**, 9381 (1990).

[23] M. J. Lighthill, *Introduction to Fourier Transform* (Cambridge University Press, Cambridge, 1958), p. 52.